Oxygen reduction reaction electrocatalytic activity of tilted pt nanorod arrays fabricated by glancing angle deposition

Wisam J. Khudhayer, Mahbuba Begum, Udaya B. Nasini, M. F. Cansizoglu, Mesut Yurukcu, Ali U. Shaikh & Tansel Karabacak

Journal of Applied Electrochemistry

ISSN 0021-891X
Volume 45
Number 10

J Appl Electrochem (2015) 45:1113-1121
DOI 10.1007/s10800-015-0871-7

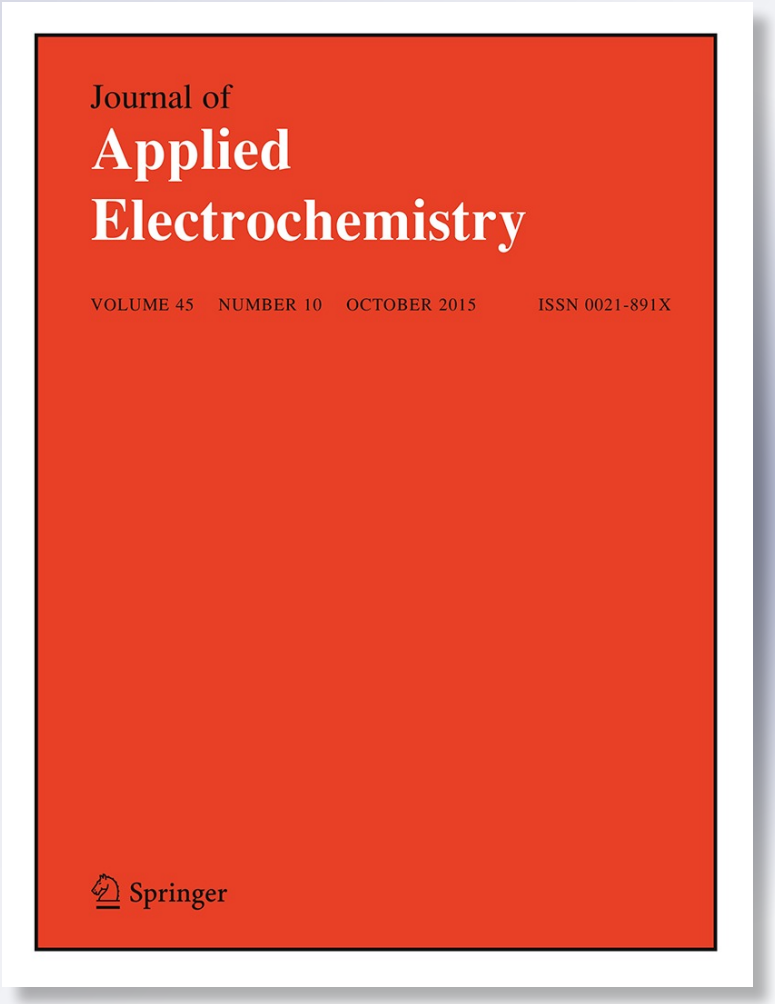

Springer

J Appl Electrochem (2015) 45:1113–1121
DOI 10.1007/s10800-015-0871-7

RESEARCH ARTICLE

Oxygen reduction reaction electrocatalytic activity of tilted pt nanorod arrays fabricated by glancing angle deposition

Wisam J. Khudhayer[1] · Mahbuba Begum[2] · Udaya B. Nasini[2] · M. F. Cansizoglu[3] · Mesut Yurukcu[3] · Ali U. Shaikh[2] · Tansel Karabacak[3]

Received: 16 March 2015 / Accepted: 29 June 2015 / Published online: 8 July 2015

Abstract Sputter glancing angle deposition (GLAD) technique was used to fabricate 50 and 200 nm long tilted Pt nanorods on glassy carbon electrodes with weight loadings of 0.042 and 0.117 mg cm^{-2}, respectively. GLAD-tilted Pt nanorod electrodes were investigated as potential electrocatalysts for proton exchange membrane fuel cells utilizing cyclic voltammetry (CV) and rotating-disk electrode (RDE) techniques in aqueous perchloric acid ($HClO_4$) to determine their oxygen reduction reaction (ORR) activities and stabilities. The CV results demonstrate that the tilted Pt nanorods electrocatalyst exhibits more positive oxide reduction peak potential compared to conventional carbon supported Pt particles (Pt/C), indicating that tilted GLAD Pt nanorods are less oxophilic than Pt/C. In addition, the multiple CV cycles in acidic electrolyte showed that tilted Pt nanorods are significantly more stable than Pt/C. Furthermore, specific ORR activities of tilted Pt nanorods determined by RDE technique were analyzed and compared to literature values of Pt/C and vertically aligned Pt nanorod electrodes. The room temperature RDE results revealed that tilted Pt nanorods demonstrate higher area-specific activity than that of Pt/C catalyst. The enhanced ORR activity of tilted Pt nanorods is due to their large crystallite size and possible dominance of the preferred crystal orientations for ORR. However, the tilted Pt nanorods showed lower mass-specific activity than Pt/C electrocatalyst caused by the large diameters of the tilted Pt nanorods. Overall ORR activity and stability of tilted Pt nanorods were found to be comparable to those of vertical ones.

Keywords Glancing angle deposition (GLAD) · Tilted Pt nanorods · Nanostructured electrocatalysts · Proton exchange membrane fuel cell (PEMFC) · Oxygen reduction reaction (ORR)

1 Introduction

Oxygen reduction reaction (ORR) limits the efficiency of the electrochemical energy conversion devices, ranging from fuel cells to metal-air batteries, due to the slow kinetics and thus it is of great interest to discover low cost, high activity, and durable electrocatalysts [1]. Proton exchange membrane fuel cells (PEMFCs) are attractive power sources for electric vehicle application because of their high-energy conversion efficiency, low operating temperature, and low emissions [2]. While the overpotential for the anodic oxidation of pure hydrogen is negligible even at high current densities due to facile H_2 oxidation kinetics on platinum (Pt), the strong inhibition of the cathodic ORR results in high overpotentials, thus requiring high Pt catalyst loadings, which increase costs [1–3]. Typical anode and cathode electrocatalyst are composed of Pt nanoparticles (3–5 nm in diameter) supported on high-surface-area carbon black (Pt/C) [2]. Besides the issues associated with Pt, there are additional performance issues related to carbon support, including oxidation of the carbon resulting in loss of Pt nanoparticles [4], formation of peroxide species leading to degradation of the polymeric

✉ Wisam J. Khudhayer
wisamjaleel@yahoo.com; met.wisam.j@uobabylon.edu.iq

[1] Department of Energy Engineering, University of Babylon, Hilla 51002, Iraq

[2] Department of Chemistry, University of Arkansas at Little Rock, Little Rock, AR 72204, USA

[3] Department of Physics and Astronomy, University of Arkansas at Little Rock, Little Rock, AR 72204, USA

membrane, and separation from the ionomer leading to loss of catalyst electrochemically active surface area (ECA) [5]. Due to these limitations, extensive efforts are focused on the development of high-performance, low-Pt-content, durable, and carbon-free catalysts with stable support materials [6–13].

The 3 M Company has demonstrated greatly enhanced activity and durability of nanostructured thin film Pt (3 M NSTF Pt) electrocatalysts composed of large-grained polycrystalline Pt or Pt alloy thin films deposited on encapsulating oriented crystalline whiskers of an organic pigment [2, 7, 13–15]. The low volume of the organic pigment catalyst support, relative to Pt/C, results in electrodes that are over an order of magnitude thinner than traditional Pt/C-based electrodes with equivalent Pt loading, which is both a benefit and challenge of this design. The challenge arises in the high volumetric rate of water production, which can lead to issues with water accumulation and freezing during transients and low-temperature start-up, respectively [16]. Another issue inherent in the NSTF electrocatalysts is the likely decomposition of the organic whisker support, which limits the thermal processing of these materials at higher temperatures [2, 7, 15]. Thermal annealing has been demonstrated to induce subsurface Pt to segregate to the surface, forming a core–shell in Pt–base metal alloy catalysts leading to enhancement of catalytic activity [17–20].

Porous nanostructured thin films with a well-controlled surface morphology can be grown using a simple physical self-assembly technique known as glancing angle deposition (GLAD) in which a vaporized particle flux arrives at the substrate from an oblique angle of incidence. During GLAD, there is a preferential growth on the islands of higher height due to a "shadowing effect" of the obliquely incident flux of atoms, which leads to the formation of isolated nanostructured geometries [21]. Bonakdarpour et al. fabricated titanium (Ti) nanocolumns on glassy carbon (GC) disks using GLAD [7]. The Ti nanocolumns were used as supports for Pt thin films deposited at a normal incidence angle ($\theta = 0°$). While the reported ORR-specific activity (500 μA cm^{-2} at 0.9 V) of these catalysts is lower than that was reported for the 3 M electrocatalyst (3 M NSTF Pt), this activity is higher than that of the conventional Pt/C electrocatalyst. On the other hand, Gasda et al. deposited platinum catalyst layers onto gas diffusion layer (GDL) substrates by GLAD and tested them as cathodes in PEFCs [8]. Their results suggest that the GLAD technique combines the advantages of thin film electrodes and the ability to fabricate porous electrodes allowing the efficient reactant flow especially for high current density operations. Gasda et al. have extended this approach to normal-incidence-angle-deposited Pt on chromium nitride (CrN) nanoparticles [9], patterned carbon nanorods [10], and electrochemically etched carbon nanorod array supports [11]. Compared to the 3 M NSTF Pt, one of the potential drawbacks of the above approaches [7–11] is that Pt tends to accumulate mainly on the tips of relatively dense nanoparticle/nanorod/nanocolumn supports, which results in lower catalyst utilization and dissolution of base metal, which in some cases can lead to complicated redox processes and deactivation of the electrode for ORR.

The design and fabrication of multicomponent nanostructures with different morphologies by GLAD have been reviewed by He and Zhao [21]. Recently, we have used the GLAD technique to grow vertically aligned Pt nanorods [13] and Pt thin films coated on Cr nanorods [2]. These nanorod structures were supported on glassy carbon for evaluation of ORR activity using the rotating-disk electrode (RDE) technique in aqueous acidic electrolyte. Our studies showed enhanced ORR activity and stability of GLAD Pt nanorods compared to conventional Pt/C catalysts. The enhanced activity was attributed to large crystallite size, single-crystal property, and the dominance of Pt$\langle 110 \rangle$ crystal planes on the nanorod sidewalls reported to be the most active face for ORR in perchloric acid electrolyte [12, 13, 17, 23]. More recently, we have also utilized GLAD technique to fabricate platinum–nickel (Pt–Ni) alloy nanorod arrays on glassy carbon electrodes [15]. The ORR mass-specific activity of the Pt–Ni alloy nanorods was found to be a factor of 2.3–3.5 higher than that of pure Pt nanorods of the same dimensions and increase with increasing Ni content, whereas ORR area-specific activity enhancement was only observed for the nanorods with the highest Pt content. In addition, the Pt–Ni alloy nanorods were found to have higher stability against loss of ECA during potential cycling than Pt nanorods and conventional high-surface-area-carbon-supported Pt nanoparticles.

By utilizing GLAD, it is furthermore possible to grow non-supported nanostructures of Pt and Pt alloys of different shapes, controllable sizes, compositions, and morphologies. This could also address some of the issues inherent in supported thin film structures (e.g., 3 M's NSTF catalysts) and also impart catalytic enhancement based on the ability to control the surface termination to the most active crystal planes for ORR. In this paper, we have used the GLAD technique to grow tilted Pt nanorod array electrocatalysts on glassy carbon substrates for the evaluation of the electrocatalytic ORR activity. Scanning electron microscopy (SEM), θ–2θ scan, and pole-figure X-ray diffraction (XRD) have been utilized to study the morphology and crystallographic structure of the tilted Pt nanorods. Cyclic voltammetry (CV) and RDE experiments were performed at room temperature in acidic medium to characterize the ORR activity and electrochemical stability of the tilted Pt nanorods.

2 Experimental work

The tilted Pt nanorods were deposited on glassy carbon (GC) inserts (5 mm OD × 4 mm thick, Pine instrument, NC) and silicon (Si) wafer pieces by DC magnetron sputter GLAD technique (Excel Instruments, India). The schematic of the GLAD experimental setup is shown in Fig. 1. The tilted Pt nanorod arrays-coated Si substrates were utilized for SEM and XRD analyses. The base pressure is 2.5×10^{-6} Torr that was achieved using a turbo-molecular pump backed by a mechanical pump. The Si and GC substrates were mounted, at the same time, on a sample holder located approximately 12 cm away from Pt target (disk-shaped source) of diameter 2.54 cm. During Pt deposition, the sputter power was 150 W with an ultrapure Argon (99.99 % purity) working gas pressure of 3.0 motor. Thickness and deposition rate of the deposited film were measured utilizing a quartz-crystal microbalance attachment (QCM, Inficon-Q-pod QCM monitor, crystal: 6 MHz gold coated standard quartz). The Pt deposition rate was further confirmed using SEM analysis to measure the length of the nanorods after various deposition times. A growth time of 6 and 24 min resulted in 50 nm and 200 nm long nanorods arrays, respectively. Pt nanorods were deposited at an oblique angle deposition of $\theta = 85°$ (with respect to substrate normal) on the substrates. For Pt loading measurements, the tilted Pt nanorods were deposited, in a separate run, directly on QCM substrate and loading values were determined by comparing the oscillation frequencies of the blank and the coated crystal.

The surface morphology of the tilted Pt nanorods was investigated using SEM analysis (FESEM-6330F, JEOL Ltd, Tokyo, Japan). Crystallographic structure of the nanorods was determined using $\theta-2\theta$ X-ray diffraction (XRD, Bruker D8 discover) and pole-figure XRD. The $\theta-2\theta$ XRD scan method is a versatile technique for the study of crystal orientations perpendicular to the substrate plane (i.e., orientation of crystal planes parallel to the substrate surface or, in other words, "texture") of thin films and nanostructured coatings. On the other hand, XRD pole-figure analysis provides information on the angular dependence of a specific crystal orientation over angles ranging from 0° (perpendicular to the substrate plane) to about 90° (parallel to the substrate plane) [13, 24, 25]. In our study, XRD pole-figures of Pt(100), Pt(110), and Pt(111) were performed using a step size of the azimuth aglen $\Delta\phi = 3°$ ($\phi = 0$–360°) and 1° for the range of χ values of 0°–50° and 60°–90°, respectively, with a step size of 10°.

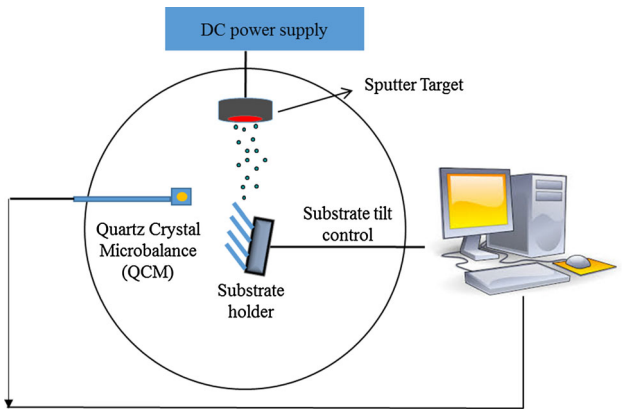

Fig. 1 A schematic of the glancing angle deposition (GLAD) technique used for the fabrication of titled Pt nanorod arrays is shown

The electrochemical measurements (CV and RDE) were performed in deaerated and oxygen-saturated 0.1 M $HClO_4$ (GFS Chemical, Inc., VERITAS double-distilled in >18 MΩ-cm^{-1} Millipore water) at room temperature for characterizing the catalyst ORR activity of the tilted Pt nanorod array electrocatalysts using a three-electrode cell and a potentiostat (Pine Instrument, bipotentiostat (AFCBP1), Raleigh, North Carolina). The electrochemical cell was composed of a working electrode of a glassy carbon disk on which tilted nanorods were deposited, a platinum wire counter electrode mounted in a separate fritted compartment, and Ag/AgCl used as reference electrode. The measured potential of this reference electrode was converted against reversible hydrogen electrode (RHE) and all potential reported in this experiment with respect to RHE. Both the nitrogen (N_2) and oxygen (O_2) gasses used were ultrahigh purity (99.99 %). An interchangeable, removable glassy carbon disk (5 mm OD × 4 mm thick) of an electrode (RDE, 6.5 mm ID, 7.5 mm OD, Pine Instruments, NC) was used as a substrate for preparing Pt nanorods electrodes. The geometric area of the glassy carbon disk-working electrode was approximately 0.196 cm^2.

For CV measurements, the working electrodes were scanned between 0.05 V and 1.4 V at a scan rate of 100 mV s^{-1} in nitrogen (99.99 % purity, Air Gas)–saturated 0.1 M $HClO_4$ to electrochemically clean (activate) the electrode surface. The activation was completed when the CV profile reached a steady state, typically after fifty cycles. The working electrodes were then scanned within the above potential range at 50 mV s^{-1} for two to three cycles to obtain CVs to be used for background subtraction and ECA determination. The working electrodes were also cycled numerous times (~2000 cycles) in the 0.6–1.4 V range at 50 mV s^{-1} to test the stability of the electrodes in the acidic environment. This test was followed by two cycles in the low potential range (0.6 to 0.05 V) to obtain the hydrogen adsorption (H_{upd}) charge used for estimating the ECA. The ECA losses were calculated by comparing the ECA values before and after the potential cycling. For

the evaluation of ORR kinetics, CVs were recorded between 0.05 and 1.4 V at a scan rate of 20 mV s^{-1} in oxygen (99.99 %, Air Gas)–saturated 0.1 M $HClO_4$ at room temperature and an electrode rotation speed of 1600 rpm. To eliminate the effect of pseudo-capacitive currents on the calculated ORR activities, the background currents obtained using nitrogen-saturated 0.1 M $HClO_4$ were subtracted from the currents obtained in oxygen-saturated electrolyte. The reported ORR activities were obtained from the positive-going potential sweep of the CVs.

3 Result and discussion

Figure 2 shows top and cross-sectional SEM images of the tilted Pt nanorod arrays of (a) 50 and (b) 200 nm in lengths. As illustrated in Fig. 2, Pt nanorod arrays deposited by GLAD technique have an isolated, tilted aligned morphology. In the initial stages of GLAD growth, the number density of the rods is large and the rods have diameters ranging from 5 to 15 nm. However, as the rods get longer, they also grow in the lateral direction to diameters up to 30 nm. During this stage, the average gap between the rods also changes with increasing length from an initial gap of 5–10 to 20–30 nm.

The structure of the 50 nm long tilted Pt nanorods seems less isolated compared to 200 nm nanorods. Figure 2a reveals that the 50 nm nanorods hardly show tilt directionality in both top and cross-sectional view SEM images. Contrary to their vertically aligned Pt nanorod counterparts [13], as they get longer, their diameters seem to stay almost constant. This means a larger surface to volume ratio can be obtained compared to vertical Pt nanorods, which can greatly enhance-mass-specific electrochemical activity. On the other hand, the gaps perpendicular to the growth direction are much smaller than the gaps in the flux direction, which reaches 100 nm lengths, as seen in Fig. 1c. This isolated nature of the rods in lateral directions leads to a channeled porosity aligned in the tilted direction to the substrate surface. This geometry can greatly help the effective transport of oxygen molecules to the catalyst sites.

A conventional QCM setup was used to measure the Pt loading of the tilted Pt nanorod samples. Using the Sauerbrey's equation:

$$\Delta f = -\frac{2f_o^2}{A\sqrt{\rho_q \mu_q}}\Delta m \quad (1)$$

where Δf is the frequency change (Hz), f_o is the resonant frequency (Hz), Δm is the mass change (g), A is the piezoelectrically active crystal area (0.3 cm^2), ρ_q is the density of quartz ($\rho_q = 2.643$ g cm^{-3}), and μ_q is the shear modulus of quartz for AT-cut crystal ($\mu_q = 2.947 \times 10^{11}$ g cm^{-1} s^{-2}). The weight loadings of 50 and 200 nm tilted Pt nanorods were measured to be about 0.042 and 0.117 mg cm^{-2}, respectively. The mass loading is an important parameter for calculating the electrochemical active surface area (ECSA) as well as the porosity of the electrodes. The porosity of Pt nanorods was calculated to be 61 and 58 % for 50 and 200 nm nanorods, respectively.

The XRD patterns of the tilted Pt nanorods deposited on Si substrates are shown in Fig. 3. It was observed that the crystal orientations of Pt nanorod arrays are quite different from that of a polycrystalline continuous film, which was deposited at normal incidence by otherwise using similar deposition conditions as the tilted Pt nanorods. The XRD results reveal that the tilted Pt nanorods have almost an even distribution of peaks along in the (111), (200), (220), and (311) directions, whereas thin film has a dominant (111) orientation. The Pt(111) is the energetically favorable growth plane of Pt films. The orientations in tilted Pt nanorods also differ from their vertical nanorod counterparts where the vertical nanorods have a tendency to grow in [200] as the nanorod length increases. The formation of energetically unfavorable texture during GLAD is believed to be due to lower adatom mobility and faster vertical growth rate of some crystal orientations. The islands of these directions can grow longer, shadowing others, and giving way to the novel texture of the Pt nanorods. Some crystal orientations have enhanced electrochemical activities compared to others, and therefore controlling of texture

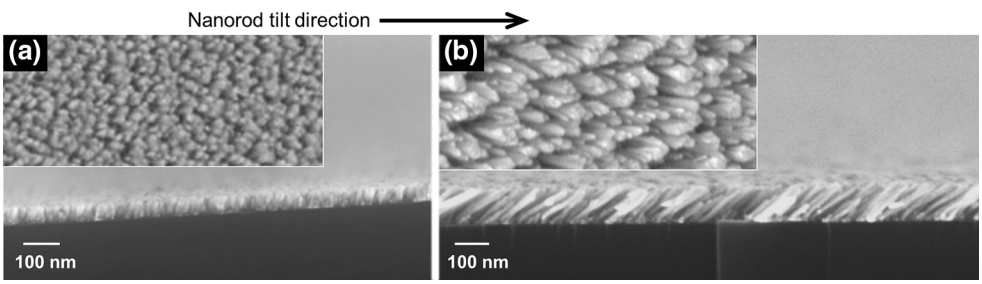

Fig. 2 Top view and cross-section SEM views of tilted Pt nanorod arrays grown at lengths of **a** 50 and **b** 200 nm

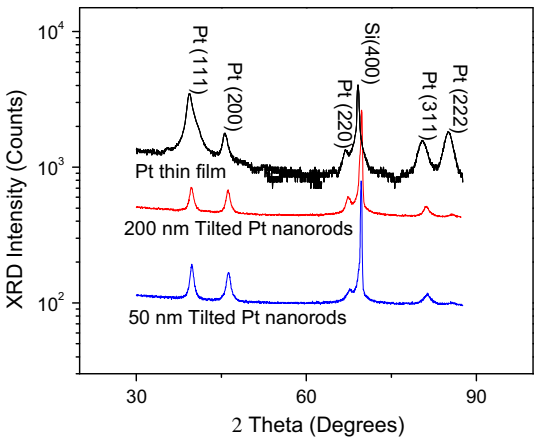

Fig. 3 X-ray diffraction (XRD) profiles of conventional Pt film, 50 nm tilted Pt nanorods, and 200 nm tilted Pt nanorods. Data is offset for clarity

may positively affect the performance of fuel cell electrodes.

In our previous study [26], we showed that GLAD Pt nanorods are highly hydrophilic enabling penetration of aqueous electrolyte and/or ionomer into the nanorod arrays, and interaction of the electrolyte with not only the tips, but also with the high-surface-area nanorod sidewalls as well. Therefore, we have measured the crystal orientations of the tilted Pt nanorods' tips and sidewalls utilizing XRD pole-figure analysis. Figure 4 shows the XRD pole-figure measurements of tilted Pt nanorods for Pt(111), Pt(100), and Pt(110) planes. From SEM images, the tilt angle of the nanorods was measured to be about 45°–55° from surface normal of the substrate. Because the Pt sputter flux is coming from right hand side in Fig. 4 (columns are tilted to the right), it was observed that there is a strong peak, which corresponds to the crystal plane Pt(111), located at $\sim 40^{\circ}$ (Fig. 4a). Since Al and Pt have both *fcc* structure, similar trend was concluded by Deniz et al. [27], who observed that the (111) peak of aluminum nitride thin films was tiled toward the incoming flux.

Based on the fact that the nanorod sidewalls take the most portion of nanorod surface area and therefore are expected to react more with the electrochemical solution compared to other portions of the nanorod, it is important to determine the crystal orientations on the nanorod sidewalls. These sidewalls face up at an angle of about $\sim 45^{\circ}$ to the left from the center of the poles (i.e., to the left along the horizontal x-axis in Fig. 4). Figures 4a and c show that there is a (110) peak close to 55° on the left and there are two (111) peaks at about $\sim 35^{\circ}$ also close to the left axis. The Pt(100) plane also has peaks at about 40° on the left half of the poles as shown in Fig. 4b, but they are farther away from the left horizontal axis. These (100) peaks are closer to the upper and

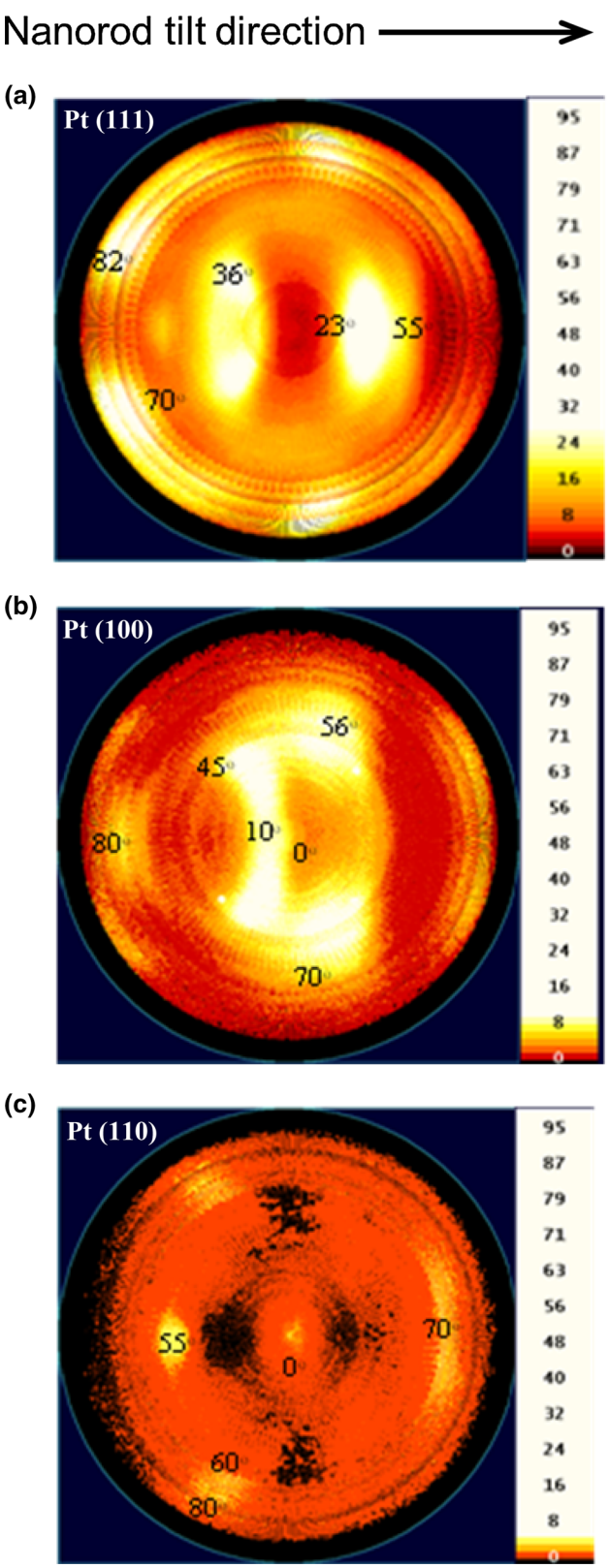

Fig. 4 XRD pole-figure results for **a** Pt(111), **b** Pt(100), and **c** Pt(110) planes for 200 nm long tilted Pt nanorods

lower portions of y-axis, which correspond to the sidewalls of the nanorods perpendicular to the incident flux direction. However, along that direction nanorods are more closely spaced (Fig. 2), which might block the easy passage of electrochemical solution. Therefore, it is believed that the crystal plane (110) and (111) are expected to dominate the electrochemical activity while (100) would be the least; (110) > (111) > (100). It was reported that the ORR electrocatalytic activity in perchloric acid electrolyte for different crystal planes of Pt follows the following trend Pt(110) > Pt(111) > Pt(100), with relative ORR activities of approximately 1.5, 1.2, and 0.6 as compared to polycrystalline Pt [13, 15], which align well with the order of existing crystal orientations in our tilted nanorods.

The CV and RDE measurements were performed on 50 and 200 nm long tilted Pt nanorods, which have Pt loading of 0.042 and 0.117 mg cm^{-2}, respectively. During CV measurement, the GLAD tilted Pt nanorod array electrodes were scanned between 0.05 to 1.4 V in oxygen-free 0.1 M $HClO_4$ at a scan rate of 50 mV s^{-1} at room temperature. The CV profile of the titled Pt nanorods shows hydrogen adsorption/desorption peaks between 0.05 and 0.4 V, the double layer capacitive current plateau (0.4–0.6 V), and the Pt hydroxide/oxide peaks (0.7–1.0 V).

These tilted nanorods exhibited adsorption and desorption of hydrogen on glassy carbon electrodes representing the presence of pure Pt surface responsible for electrocatalytic reactions. Generally, the peaks at approximately 0.11 V can be assigned to (110) and at 0.2–0.4 V to (100) surfaces, while the (111) terraces give a constant H_{upd} current over this region. As shown in the CV for the titled Pt nanorods in O_2-free electrolyte, the tilted Pt nanorods have an oxide-reduction peak potential of 0.82 V. This potential is 40 mV more positive than the oxide reduction peak observed for Pt/C [13], indicating that the tilted Pt nanorods are less oxophilic than Pt/C. On the other hand, it is nearly identical to the peak potential for oxide reduction of vertically aligned GLAD Pt nanorods as well as polycrystalline Pt [13].

The ECA of the tilted Pt nanorods was determined by integrating the charge in the hydrogen adsorption region derived from CV profiles between the double layer region and the onset of hydrogen evolution, after subtracting the double layer charging current, and using the following equation to convert this charge to ECAs [1]:

$$\mathrm{ECA}_{\mathrm{Pt,cat}}(m^2 g_{\mathrm{Pt}}^{-1}) = \left[\frac{Q_{\mathrm{H-Adsorption}}(C)}{210\mu C \mathrm{cm}_{\mathrm{Pt}}^{-2} L_{\mathrm{Pt}}(\mathrm{mg_{Pt}cm^{-2}})\mathrm{A_g(cm^2)}}\right] 10^5 \quad (2)$$

where Q_H (210 μC cm^{-2}) is the charge of full coverage for clean polycrystalline Pt, $L_{Pt,cat}$ is the working electrode Pt loading (mg_{Pt} cm^{-2}), and A_g is the geometric surface of the GC electrode (0.196 cm^2). The results show that the ECAs of 50 and 200 nm long tilted Pt nanorods with Pt loadings of 0.042 and 0.117 mg cm^{-2} are 14.6 and 14.9 m^2 g^{-1} Pt, respectively (Table 1). In contrast to our observations on vertically aligned Pt nanorods [13], which showed a decrease in ECA with increasing nanorod length, the relatively close values of ECA of the 50 and 200 nm tilted Pt nanorods indicate their enhanced wetting property compared to vertical nanorods (Fig. 5).

The 50 and 200 nm long tilted Pt nanorod electrodes were scanned multiple times O_2-free 0.1 M $HClO_4$ in the potential range of 0.6–1.4 V at a scan rate of 50 mV s^{-1} to evaluate the potential durability of the tilted Pt nanorod electrodes during PEMFC load cycling. Figure 6 reveals that the 50 and 200 nm long Pt nanorods retained 76 and 80 % of their initial ECAs, respectively. These results indicate that the tilted Pt nanorods are more stable than Pt/C electrode during potential region and acidic environment relevant to the PEMFC cathode. The electrochemical stability of the tilted Pt nanorods is almost similar to their vertical nanorod counterparts [13].

The ORR activity of the tilted Pt nanorod electrodes was determined using the RDE technique and CVs taken at 20 mV s^{-1} in O_2-saturated 0.1 M $HClO_4$ electrolyte. The anodic-going traces of these CVs are shown in Fig. 7. The onset of the ORR occurred at 1.06 V and the CVs exhibit the typical mixed kinetic-diffusion controlled region from 0.8 to 1.0 V and diffusion-limited current region from 0.2 to 0.8 V. The diffusion-limited current densities for 50 and 200 nm tilted Pt nanorod electrodes, normalized to geometric surface area of the RDE tip, are within 10 % of the theoretical diffusion limiting current (5.7 mA cm^{-2}) expected for a rotation rate of 1600 rpm, O_2-saturated room temperature electrolyte, and a four-electron reduction [15]. This agreement indicates uniform and complete coverage of the GC disks with catalyst and minimal effects of inhibition of oxygen diffusion through the thickness of the nanorod layer [1, 3, 28]. It should be noted that the relatively lower diffusion limiting current for 50 nm long tilted Pt nanorods may be attributed to the much lower Pt loading (0.042 vs 0.117 mg_{Pt} cm^{-2}) leading to reduced coverage of the glassy carbon disk with nanorods.

The ORR electrocatalytic activities of the tilted Pt nanorod electrodes are reported as area-specific (SA) and mass-specific (MA) activities extracted from the background-corrected RDE profiles using the well-known mass-transport correction for RDE measurements [3, 28, 29]:

$$\frac{i_k = (i_{\mathrm{lim}} \times i)}{(i_{\mathrm{lim}} - i),} \quad (3)$$

where i is the measured current at a specified potential, i_{lim} is the measured limiting current, and i_k is the kinetic

Table 1 Summary of the evaluated electrocatalytic activity (area-specific and mass-specific activities at 0.90 V) of tilted Pt nanorods catalyst with different lengths in 0.1 M $HClO_4$ and comparison to the literature values for various Pt-based catalysts

Method	Sample	Pt loading (mg cm^{-2})	ECA (m^2 g^{-1})	T (°C)	Scan rate (mV s^{-1})	SA (μA cm^{-2}) 0.90 V	MA (A mg^{-1}) 0.90 V	Ref.
RDE	50 nm long tilted Pt nanorods	0.042	14.6	25	20	810	0.120	This work
RDE	200 nm long tilted Pt nanorods	0.117	14.9	25	20	715	0.106	This work
RDE	50 nm long vertical Pt nanorods	0.040	13.0	20	10	632	0.080	[13]
RDE	200 nm long vertical Pt nanorods	0.160	12.0	20	10	1080	0.130	[13]
TF-RDE	20 % Pt/C	0.020	60.0	20	20	288	0.180	[13]

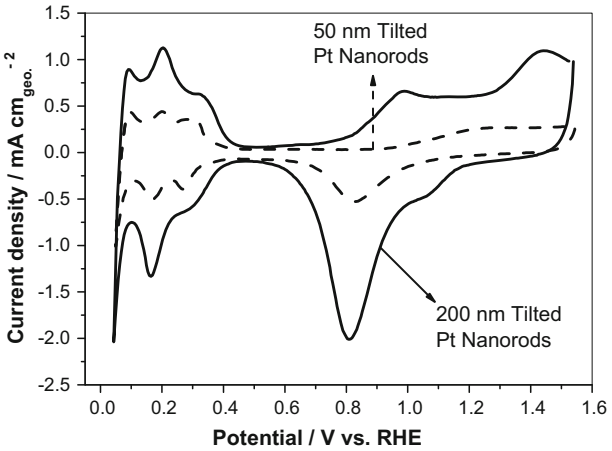

Fig. 5 Room temperature CVs in O_2-free 0.1 M $HClO_4$ at a scan rate 50 mV s^{-1} of 50 and 200 nm long tilted Pt nanorods, which correspond to Pt loading of 0.042 and 0.117 mg cm^{-2}, respectively

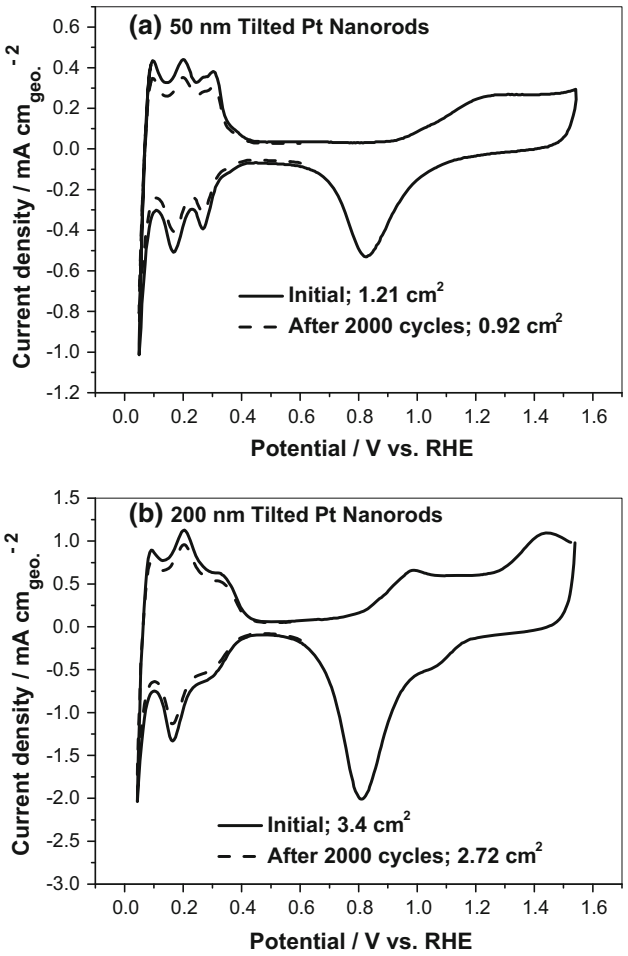

Fig. 6 Room temperature CVs of **a** 50 and **b** 200 nm long tilted Pt nanorods over first cycle and 2000 cycles at scan rate of 50 mV s^{-1}. Data were recorded in O_2-free 0.1 M $HClO_4$

current. The assumptions for extracting i_k from the RDE data using Eq. (3) are valid over the current range of 0.1 $i_{lim} < i < 0.8\ i_{lim}$ [3]. Specific activities can be determined by calculation of i_k using Eq. (3) and normalization to measured Pt ECA and Pt loading. The area- and mass-specific activities for 50 and 200 nm long tilted Pt nanorods at 0.9 V are reported in Table 1. It was found that the 50 nm tilted Pt nanorod electrode exhibits higher *SA* and *MA* than those of 200 nm long tilted Pt nanorod electrode. The lower SA and MA activities of 200 nm tilted Pt nanorods are caused by the larger diameters and incomplete wetting compared to shorter nanorods. This observation is also supported by the ECA calculation shown above. The other reason may be attributed to the fact that the enhancement of ORR activity is a function of the relative abundance of active surface Pt planes as discussed above in analyzing XRD pole-figure.

The reported values of SA and MA activities at 0.9 V taken from literature [13] for vertically aligned Pt nanorods and Pt/C electrodes are also reported in Table I for comparison. The higher SA activity of tilted Pt nanorods compared to Pt/C electrode has been attributed to the large Pt crystallite size resulting in average coordination numbers of surface Pt and corresponding surface electronic properties approaching those of polycrystalline [3].

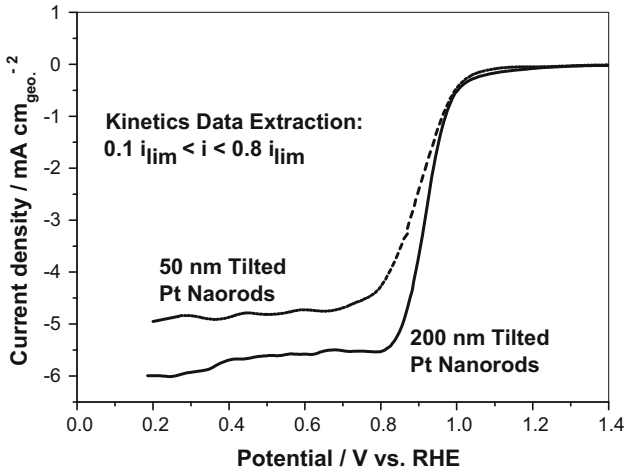

Fig. 7 Room temperature RDE profiles of 50 nm and 200 nm tilted Pt nanorods in oxygen-saturated 0.1 M $HClO_4$ at a scan rate of 20 mV s^{-1} and rotation speed of 1600 rpm

However, the large crystallite size of the tilted Pt nanorods catalysts results in a lower ratio of surface to bulk Pt atoms and a concomitantly lower MA activity than Pt/C catalyst as shown in Table 1 (It should be noted that the average nanorod diameter, which was estimated from SEM analysis, is referring to an approximate crystallite size). In our previous work [13], we concluded that both a catalyst loading that is too high (400 nm long vertically aligned Pt nanorods) as well as too low (50 nm long vertically aligned nanorods) must be avoided; the 200 nm long Pt nanorods showed better ORR electrocatalytic activity. While, the 50 nm long tilted Pt nanorods showed higher SA and MA activities compared to 200 nm tilted Pt nanorods as well as their 50 nm long vertically aligned Pt nanorod counterparts. It is also comparable to the activity of 200 nm long vertically aligned Pt nanorods with relatively lower SA. The ORR activity enhancement of 50 nm tilted Pt nanorods may be attributed to the enhanced roughness of the single nanorod and possibly a preferential exposure of certain crystal facets. On the other hand, the incomplete wetting of the nanorods due to the poorer porosity as shown in the SEM images (Fig. 2) compared to 50 nm tilted Pt nanorods as well as 200 nm vertical Pt nanorods possibly causes the poorer electrocatalytic activity of 200 nm tilted Pt nanorods.

4 Conclusion

Tilted Pt nanorod arrays were grown on glassy carbon electrodes using a magnetron sputtering GLAD technique. The electrocatalytic activities for the ORR in PEMFC s on tilted Pt nanorods were investigated using CV and RDE techniques in aqueous perchloric acid electrolyte. The tilted Pt nanorods were found to have higher stability against loss of ECA during potential cycling than conventional high-surface-area-carbon-supported Pt nanoparticles (Pt/C); however, it is comparable with the stability of the vertically aligned Pt nanorod counterparts. The area-specific activities of tilted Pt nanorods were found to be higher than that of Pt/C due to their larger crystallite size and possible existence of the preferred Pt crystal planes such as Pt(110). However, the tilted Pt nanorods exhibit lower mass-specific activity than that of Pt/C catalyst, mainly due to the large diameter of nanorods. This work shows that the unsupported nanostructures produced by GLAD technique have the potential to further enhance the mass-specific activity toward ORR in fuel cells by controlling the area density, spacing, nanorod diameter, and crystallographic orientation.

Acknowledgments This work was financially supported by the National Science Foundation under grant numbers: EPS-1003970 and 1159830. The authors would like to thank the UALR Nanotechnology Center and Dr. Fumiya Watanabe for his valuable support and discussions during SEM and XRD measurements.

References

1. Garsany Y, Baturina OA, Swider-Lyons KE, Kocha SS (2010) Anal Chem 82:6321
2. Khudhayer WJ, Kariuki N, Myers DJ, Shaikh AU, Karabacak T (2012) J Electrochem Soc 159(6):B729–B736
3. Mayrhofer KJJ, Strmcnik D, Blizanac BB, Stamenkovic V, Arenz M, Markovic NM (2008) Elcetrochimica Acta 53:3181–3188
4. Tang H, Qi ZG, Ramani M, Elter JF (2006) J Power Sources 158:1306
5. Qiao JL, Saito M, Hayamizu K, Okada TJ (2006) J Electrochem Soc 153:A967
6. Debe MK, Schmoeckel AK, Hendricks SM, Vernstrom GD, Haugen GM, Atanasoski RT (2006) ECS Trans 1(8):51
7. Bonakdarpour A, Fleischauer MD, Brett MJ, Dhan JR (2008) Appl Catal A 349:110
8. Gasda MD, Teki R, Lu T-M, Koratkar N, Eisman GA, Gall D (2009) J Electrochem Soc 156(5):B614
9. Gasda MD, Eisman GA, Gall D (2010) J Electrochem Soc 157(1):B71
10. Gasda MD, Eisman GA, Gall D (2010) J Electrochem Soc 157(1):B113
11. Gasda MD, Eisman GA, Gall D (2010) J Electrochem Soc 157(3):B437
12. Khudhayer WJ, Shaikh AU, Karabacak T (2011) Adv Sci Lett 4:3551
13. Khudhayer WJ, Kariuki N, Wang X, Myers DJ, Shaikh AU, Karabacak T (2011) J Electrochem Soc 158(8):B1029
14. Debe MK, Steinbach AJ, Vernstrom GD, Hendricks SM, Kurkowski MJ, Atanasoski RT, Kadera P, Stevens DA, Sanderson RJ, Marvel E, Dahn JR (2011) J Electrochem Soc 158:B910–B918
15. Kariuki N, Khudhayer WJ, Karabacak T, Myers DJ (2013) ACS Catal 3:3123–3132
16. Steinbach AJ, Debe MK, Pejsa MJ, Peppin DM, Haug AT, Kurkowski MJ, Hendricks SM (2011) ECS Trans 41:449–457

17. Stamenkovic VR, Fowler B, Mun BS, Wang GF, Ross PN, Lucas CA, Markovic NM (2007) Science 315:493–497
18. Wang C, Chi MF, Wang GF, van der Vliet D, Li DG, More K, Wang HH, Schlueter JA, Markovic NM, Stamenkovic VR (2011) Adv Funct Mater 21:147–152
19. Wadayama T, Todoroki N, Yamada Y, Sugawara T, Miyamoto K, Iijama Y (2010) Electrochem Commun 12:1112–1115
20. Van der Vliet DF, Wang C, Tripkovic D, Strmcnik D, Zhang XF, Debe MK, Atanasoski RT, Markovic NM, Stamenkovic VR (2012) Nat Mater 11:1051–1058
21. Karabacak T, Wang GC, Lu TM (2004) J Vac Sci Technol, A 22:1778–1784
22. He YP, Zhao YP (2011) Nanoscale 3:2361–2375
23. Markovic NM, Ross PN (2002) Surf Sci Rep 45:121–229
24. Nagao K, Kagami E (2011) The Rigaku J 27(2):6–14
25. Seo K, Zhao X, Krishnan M, Bures B, Wilson K Proceedings of SRF2009, Berlin, pp 418–421
26. Khudhayer WJ, Sharma R, Karabacak T (2009) Nanotechnology 20:275302
27. Deniz D, Harper JME, Hoehn JW, Chen F (2007) J Vac Sci Technol, A 25:1214
28. Gasteiger HA, Kocha SS, Sompalli B, Wanger FT (2005) Applied Catal B 56:9–35
29. Paulus UA, Schmidt TJ, Gasteiger HA, Behm RJ (2001) J Electroanal Chem 495:134–145